Article

Seasonal Urban Heat Island observation from Remote Sensing by using Google Earth Engine over new capital (IKN) East Kalimantan, Indonesia

Laras Tursilowati [1,*], Rachmat Sunarya [1], Muzirwan Muzirwan [1], Indah Susanti [1], Soni Aulia Rahayu [1], Tatik Kartika [1], Mamat Suhermat [1], Jamrud Aminuddin [2] and Nursida Arif [3]

[1] National Research and Innovation Agency (BRIN); Bandung 40135, Indonesia; rrla001@brin.go.id
[2] Universitas Jenderal Soedirman; Purwokerto 53122, Indonesia; jamrud.aminuddin@unsoed.ac.id
[3] Universitas Negeri Yogyakarta; Yogyakarta 55281, Indonesia; nursida.arif@uny.ac.id
* Correspondence: rrla001@brin.go.id; Tel.: +62-8122007705

Abstract: The relocation of the Indonesian capital from Jakarta to Ibu Kota Nusantara (IKN) East Kalimantan IKN will affect several sectors. The change in land use from vegetated to developed land will lead to local climate changes, including the emergence of the urban heat island (UHI) phenomenon, which is reflected in a higher land surface temperature (LST) than the surrounding area. In this study, an analysis of UHI propagation was conducted on a seasonal (DJF, MAM, JJA, and SON), with 5 yearly periods from 2001 to 2020, study area in IKN and its buffer cities (Balikpapan, Samarinda, and Bontang). Terra-MODIS satellite data are processed using Google Earth Engine (GEE) platform and output is done using GrADS. UHI (high LST) is found in urban areas/buffer cities both spatially and temporally in every season, while UHI has not yet occurred in IKN (low LST) and suburban, rural, hilly areas, vegetated areas, and water bodies (lakes, rivers). The cross-sectional latitudinal and longitudinal analysis showed that the LST DJF2015-2020 from highest to lowest temperature are in Balikpapan City (36.84 ^{O}C), Samarinda City (36.13 ^{O}C), Bontang City (32.3 ^{O}C); and IKN zero point (28.82 ^{O}C). The UHI propagation was observed in 2001-2005, 2006-2010, 2011-2015, and most during 2016-2020. Seasonally, the UHI was most pronounced in the SON season, while on lowest UHI was observed in the MAM season.

Keywords: Ibu Kota Nusantara (IKN); urban heat island (UHI); land surface temperature (LST); seasonal; Terra-MODIS; Google Earth Engine (GEE), buffer cities

1. Introduction

The Indonesian government plans to relocate the Indonesian capital from Jakarta to Ibu Kota Nusantara (IKN) in Penajam Paser Utara (PPU) East Kalimantan starting in 2024. The urgency of relocating the capital is due to the objective condition of Jakarta which is no longer suitable as the capital. This is evident from "burden" Jakarta has to bear: 1) a population density of 16,704 people/km^2, while Indonesia's population density is only 141 people/km^2; 2) the traffic congestion of Jakarta, which is the number 10 most congested city in the world in 2019, although in 2020 it is only 31st out of 416 major cities in 57 countries (TomTom Traffic Index); 3) acute environmental and geological problems such as flooding that afflicts Jakarta every year and land subsidence that causes parts of Jakarta to be below sea level [1]. The location of the IKN is also said to be ideal because it is close to developed urban areas as buffer cities, namely Balikpapan, Samarinda, and Bontang. The IKN is also a national identity that is a benchmark for a smart, green, beautiful, and modern sustainable capital city with international standards.

The relocation of the capital will certainly entail massive construction works that will affect several sectors. This will greatly change the natural conditions in the surrounding area, affecting climate change and the environment. A strategic intervention program that can respond to the challenges of IKN development is the concept of Forest City and

Preprints (www.preprints.org) | NOT PEER-REVIEWED | Posted: 30 May 2023 doi:10.20944/preprints202305.2099.v1

Climate Plus Village (Proklim+). To support the concept of IKN becoming a smart metropolis that guarantees the highest quality of life for its inhabitants, climate and environmental conditions must be maintained.

Anthropogenic activities (land use and land cover change/LULC) alter the surface radiation balance so that surface temperature increases. This is known as the urban heat island (UHI) phenomenon [2,3]. UHI is a phenomenon in which urban areas have higher temperatures than suburban and rural areas. The high land surface temperature (LST) in urban areas is a manifestation of UHI, which gradually decreases in vegetated rural areas [4,5,6]. The modification of LU by adding urban in vegetation areas using Weather Research Forecasting (WRF) will increase air temperature in Jakarta and IKN [7,8].

Research on UHI and land cover using Google Earth Engine (GEE) has been studied by remote sensing experts [9–13]. GEE is a platform that is a powerful application for using big data because it does not require local storage of imagery, but allows the analysis of the satellite imagery in cloud-based processing.

2. Materials and Methods

2.1. Study Area

The location of the study area is centered on the future IKN and the surrounding area as a buffer city is located between latitudes 1.56°S – 0.26°N and longitudes 115.6°E – 117.8°E (Figure 1). The IKN is located in Samboja and Sepaku districts, North Penajam Paser Regency (PPU), East Kalimantan province with a total area of 2560 km² which is four times larger than Jakarta (661.5 km²). There are four buffer cities for IKN, namely Bontang, Samarinda, Balikpapan, and Tenggarong. Samarinda, the capital of East Kalimantan will be the "heart" as the historical center of East Kalimantan in the renewable energy sector. Balikpapan, on the other hand, is the "muscle", that will act as the downstream oil and gas hub and logistics center for East Kalimantan. The site where the IKN will be built is currently planted with *Acacia mangium* and *Eucalyptus sp.* Which are used to produce paper raw materials.

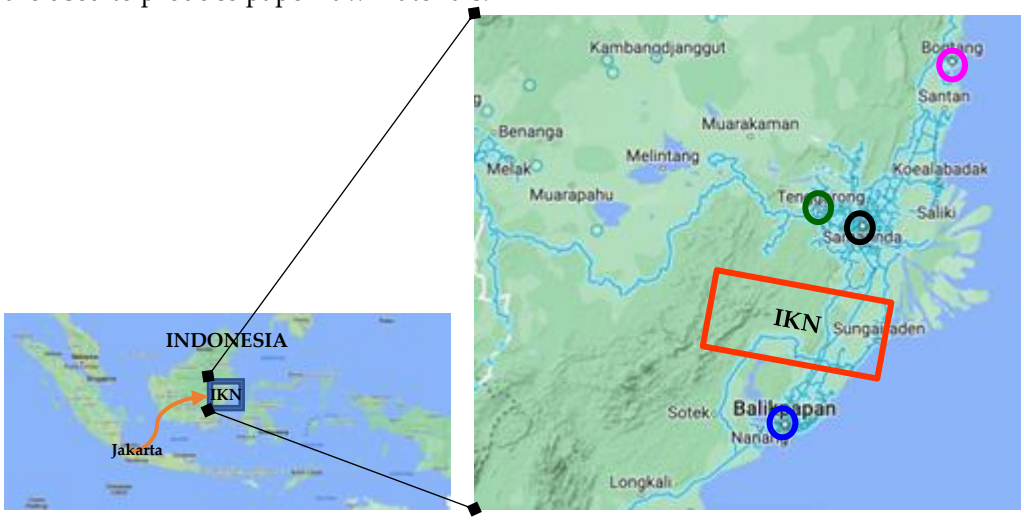

Figure 1. The study area is IKN (red square) and the surrounding area, East Kalimantan, Indonesia. Four cities as buffer cities are Bontang City (purple circle), Samarinda City (black circle), Tenggarong City (green circle), and Balikpapan City (blue circle).

East Kalimantan is located at an elevation of 0-6, 4.49 m above sea level, and has a tropical rainforest climate (Af classification according to Kopen and Geiger). East Kalimantan has an annual high temperature of 30.46 °C and an annual low temperature of 25.11 °C, the warmest month in October (30.96 °C) and the coldest month in July (24.79 °C), an average annual rainfall of 97.22 mm, and a humidity of 78.32% [14–17].

2.2. Data

Preprints (www.preprints.org) | NOT PEER-REVIEWED | Posted: 30 May 2023 doi:10.20944/preprints202305.2099.v1

This study uses the Terra Moderate Resolution Imaging Spectroradiometer (MODIS) LST and Emissivity daily (MOD11A1) version 6.1. This product provides daily LST per pixel with a spatial resolution of 1 km in a 1.200 by 1.200 km grid. The MOD11 Level 2 swath product derives the pixels LST [18].

LST Level 3 Daily is a daily LST product represented in an integrated sinusoidal projection (in V3) or sinusoidal projection (in V4). The MYD11A1 LST daily product is created from the MOD11_L2 product yields per day using scientific datasets (SDS), mapping all MOD11L2 product pixels to the grid/pixel in a sinusoidal or generated sinusoidal projection and averaging the values in each grid [19,20]. The data trimmed by the MODIS sensors cover the study area at latitude 1.56°S to 0.26°N and longitude 115.6°E to 117.8°E. The data consists of 354 columns x 138 rows (note: only 210 pixels in the 138th row) corresponding to a total area of 48,708 pixels (km^2) consisting of 36,435 km^2 of land and 12,273 km^2 of sea, the elevation following topography. The data period is from 1 January 2001 until 31 December 2020. The data format is HDF Network Common Data Form [21].

2.3. Methods

Processing MODIS data using Javascript in Google Earth Engine (GEE) platform. GEE is a cloud platform with huge data collections of remote sensing satellite imagery and geospatial data, where the process of remote sensing imagery acquisition and data processing is performed online using Javascript syntax language. Cloud computing at GEE enables faster and easier data acquisition and processing. Remote sensing image data is "called" according to the study area, processed as needed, and the processing results can be downloaded for further analysis, with a much smaller amount of data compared to conventional processing. The capability of GEE is very important at this time, especially for rapid data analysis and monitoring.

In this study, UHI was monitored based on seasonality, in December, January, February (DJF), March, April, May (MAM), June, July, August (JJA), and September, October, November (SON). Seasonal data were set as input data in GEE. The data were calculated for a 5-year average, namely, the average of 2001-2005, 2006-2010, 2011-2015, and 2016-2020, resulting in 16 files in GeoTIFF format. Figure 2 shows an example of the Javascript syntax for data processing in GEE in the period DJF 2001-2005.

```
var boundary = geometry2;
var datasetDJF = ee.ImageCollection('MODIS/061/MOD11A1')
                  .filter(ee.Filter.date('2001-01-01', '2005-12-31'))
                  .filter(ee.Filter.calendarRange(12,2,'month'))
                  .select('LST_Day_1km')
                  .mean().multiply(0.02)
                  .clip(boundary);

//var landSurfaceTemperature = datasetDJF.select('LST_Day_1km');
var landSurfaceTemperatureVis = {
  min: 273,
  max: 310,
  palette: [
    '040274', '040281', '0502a3', '0502b8', '0502ce', '0502e6',
    '0602ff', '235cb1', '307ef3', '269db1', '30c8e2', '32d3ef',
    '3be285', '3ff38f', '86e26f', '3ae237', 'b5e22e', 'd6e21f',
    'fff705', 'ffd611', 'ffb613', 'ff8b13', 'ff6e08', 'ff500d',
    'ff0000', 'de0101', 'c21301', 'a71001', '911003'
  ],
};
Map.setCenter(120, 0, 4);
Map.addLayer(
    datasetDJF, landSurfaceTemperatureVis,
    'Land Surface Temperature');

Export.image.toDrive({
  image: datasetDJF,
  description: 'LSTDJF01-05',
  region: boundary,
  fileFormat: 'GeoTIFF',
  scale : 1000
});
```

Figure 2. Javascript syntax in GEE for data processing in December-January-February 2001-2005.

In Figure 2 "Geometry 2" is the trimmed study area boundary, "Filter data" is the period from 1 January 2001 to 31 December 2005, and "calendar range" is month 12 (December) to 2 (February). When this syntax is executed, it will produce an output file named LSTDJF01-05 generated in GeoTIFF format. For other running periods and seasons, replace "filter date", "calendarRange", "dataset", and "description" according to the desired period and season.

Preprints (www.preprints.org) | NOT PEER-REVIEWED | Posted: 30 May 2023 doi:10.20944/preprints202305.2099.v1

The output of the running data from GEE (GeoTIFF format) is converted to Network Common Data Form (NetCDF or nc) format using QGIS software. NetCDF is a software library that set data and machine-independent data formats that support access, creation, and sharing of array-oriented scientific data [18]. QGIS is a freely available software and open-source application for cross-platform desktop geographic information systems (GIS) that supports editing, viewing, printing, and analyzing of geospatial data. The post-processing output data GEE runs (NetCDF data format) use Grids Analysis Display System (GrADS) (GrADS). GrADS is an easy-to-use, interactive desktop tool that is freely distributed and used to manipulate and visualize geoscience data [22].

3. Results

3.1. LST Seasonal Spatially analysis

3.1.1. LST Seasonal Spatially analysis

UHI propagation was observed through visualization of the output data spatially as shown in Figure 3. Seasonal LST DJF 2001-2005 is shown in Figure 3 (a), then LST DJF 2006-2006 in Figure (b) DJF 2006-2010, (c) DJF 2011-2015, (d) DJF 2016-2020, (e) MAM 2001-2005), (f) MAM 2006-2010, (g) MAM 2011-2015, (h) MAM 2016-2020, (i) JJA 2001-2005, (j) JJA 2006-2010, (k) JJA 2011-2015, (l) JJA 2016-2020, (m) SON 2001-2005, (n) SON 2006-2010), (o) SON 2011-2015, and (p) SON 2016-2020. Purple to red colors in the legend represent LST from low (≤22 OC) to high ((≥32 OC).

In Figure 3(a) (DJF 2001-2005), it can be seen that the areas of high temperature (≥32 ^{O}C) in urban areas shown in red, namely Bontang City (purple circle), Samarinda City (black circle), Tenggarong City (green circle), and Balikpapan City (blue circle). This high temperature reflects the occurrence of UHI. While the blue color (at LST around 22 – 25 ^{O}C) is found in suburban, rural, hilly/vegetated areas (including areas designed as IKN/red circle) and water bodies (rivers and lakes). High-temperature areas (UHI) are increasingly spreading, as shown in Figure 3(b) (DJF 2006-2010), Figure 3(c) (DJF 2011-2015), and Figure 3(d) (DJF 2015-2020). The next season is MAM, Figure 3(e) MAM 2001-2006 shows UHI in urban areas similar to the pattern in Figure 3(a) DJF 2001-2006, also Figure 3(f) is similar to Figure 3(b), 3 (g) is similar to 3(c), and 3(h) is similar to 3(d). The widest UHI occurred in 2015-2020, for both DJF and MAM.

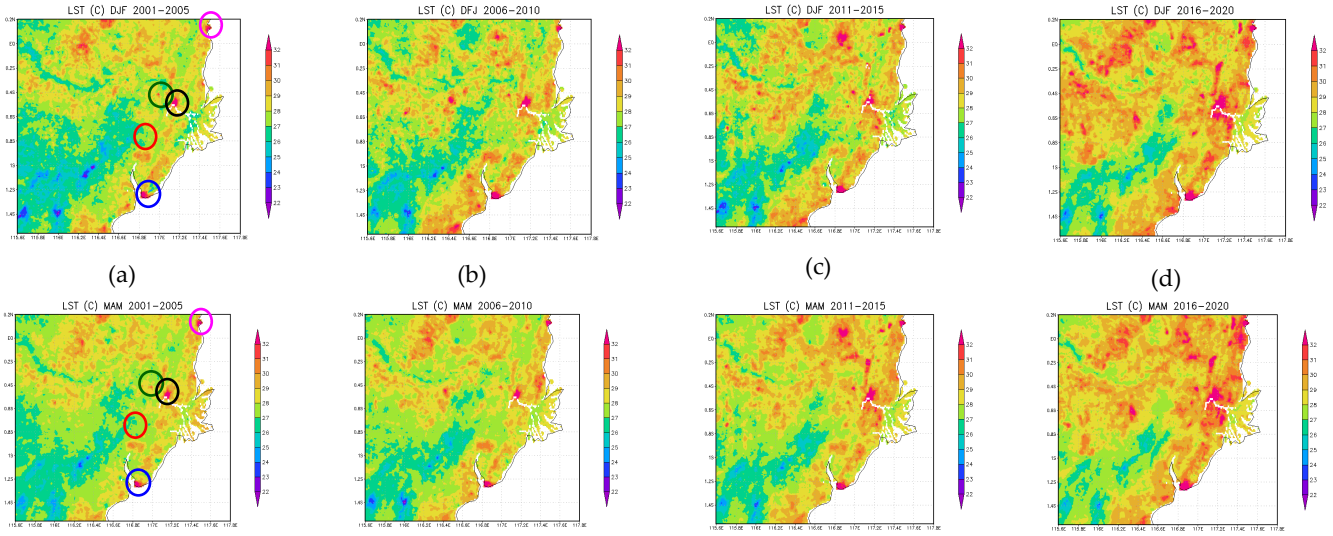

(a) (b) (c) (d)

(e) (f) (g) (h)

Preprints (www.preprints.org) | NOT PEER-REVIEWED | Posted: 30 May 2023 doi:10.20944/preprints202305.2099.v1

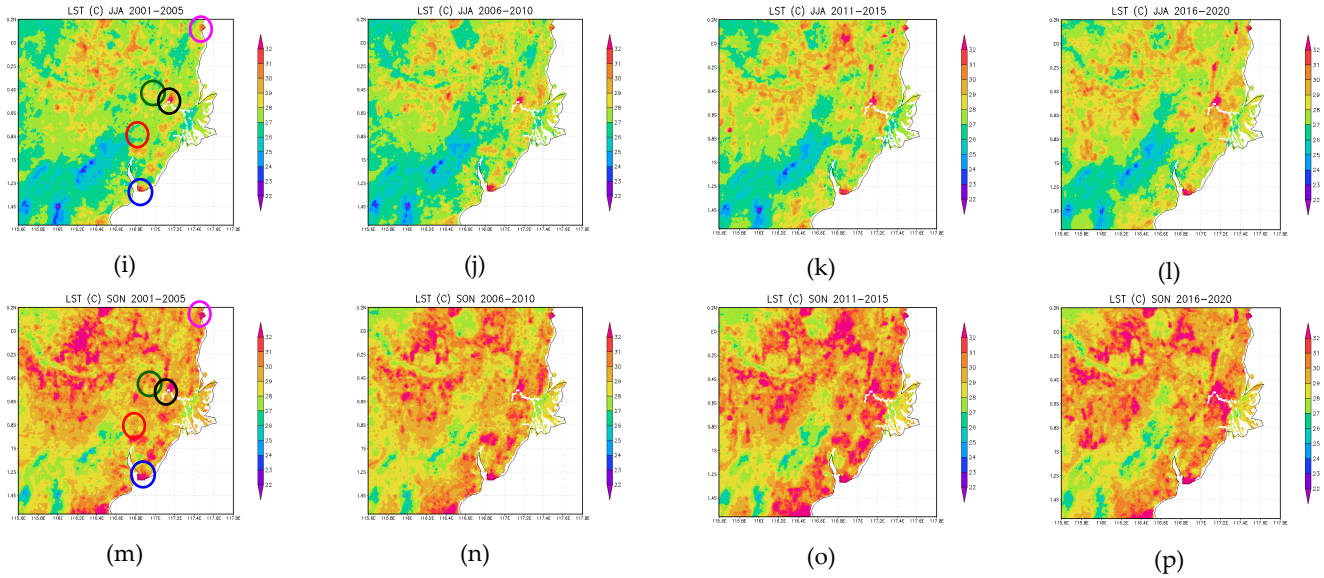

Figure 3. LST Seasonal IKN, (a) DJF 2001-2005, (b) DJF 2006-2010, (c) DJF 2011-2015, (d) DJF 2016-2020, (e) MAM 2001-2005), (f) MAM 2006-2010, (g) MAM 2011-2015, (h) MAM 2016-2020, (i) JJA 2001-2005, (j) JJA 2006-2010, (k) JJA 2011-2015, (l) JJA 2016-2020, (m) SON 2001-2005, (n) SON 2006-2010), (o) SON 2011-2015, and (p) SON 2016-2020.

The JJA season in Figure 3(i, j, k, l) shows a decrease in UHI compared to the previous season (MAM). If this is related to the monthly temperatures of East Kalimantan in Figure 4, it is reasonable. Figure 4 shows the average monthly temperature in East Kalimantan from observational data. The lowest temperature is in July and the highest is in October [12–15]. Moreover, the season SON in Figure 3(m,n,o,p) shows the highest UHI among the other seasons, even the season SON 2001-2005 (Figure 3(m)) has a higher temperature than the other seasons (DJF, MAM, JJA) in 2016-2020 (Figure 3(d, h, l)). This corresponds to Figure 4, where the highest temperatures in East Kalimantan occur in season SON season, and the lowest temperatures in season JJA.

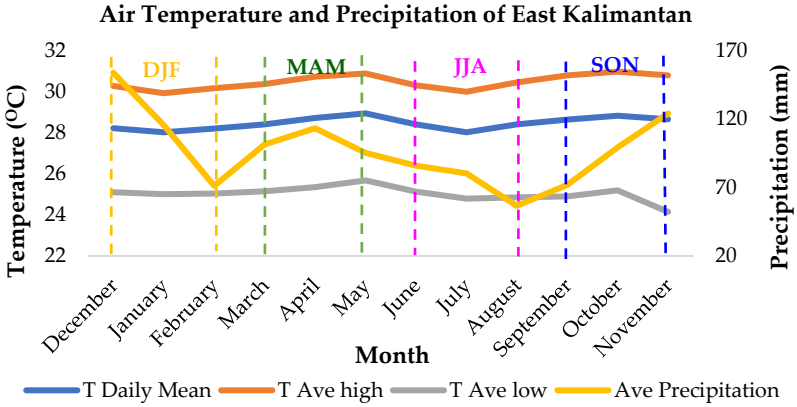

Figure 4. Monthly maximum air temperature (°C) 2019-2020 in Samarinda and Balikpapan, East Kalimantan [14, 15, 16, 17]

3.1.2. LST Statistical analysis

3.1.2.1. LST (°C) and area of LST (km²) seasonally

To find out how many temperature areas there are in each season and year, a statistical analysis of LST is performed as shown in Table 1 and Figure 4. Table 1 shows the region with temperatures from ≤ 23 to ≥ 34, and the graph is shown in Figure 5. The area of DJF 01-05 in Table 1 and Figure 4 is the quantitative value of DJF 2001-2005 LST spatial map in Figure 3(a), the area of DJF 06-10 is the quantitative value of 2006-2010 LST in Figure 3(b), and so on to SON 16-20 as the representation of LST SON 2016-2020 in Figure 3(p).

Preprints (www.preprints.org) | NOT PEER-REVIEWED | Posted: 30 May 2023 doi:10.20944/preprints202305.2099.v1

Table 1. LST (°C) and area of LST (km²) Seasonal

LST (°C)	AREA OF LST SEASONAL (km²)															
	DJF 01-05	DJF 06-10	DJF 11-15	DJF 16-20	MAM 01-05	MAM 06-10	MAM 11-15	MAM 16-20	JJA 01-05	JJA 06-10	JJA 11-15	JJA 16-20	SON 01-05	SON 06-10	SON 11-15	SON 16-20
≤ 23	39	4	21	1	0	11	6	2	28	26	22	1	0	0	0	2
24	134	59	92	24	24	51	23	3	139	117	74	58	3	1	2	1
25	430	281	329	122	206	195	154	47	631	664	580	445	62	18	28	7
26	2686	1330	1599	606	1115	779	849	391	2415	2836	2083	1729	180	82	120	123
27	7954	6365	5879	2992	6981	5131	4250	2117	9169	10154	7075	5591	622	681	773	876
28	11589	12394	10592	6531	13962	13777	10427	7224	14960	13118	12420	12128	3702	4426	3939	3712
29	10008	9758	9542	11089	10402	10860	11535	11434	6618	7061	9021	10919	10203	10915	8252	9116
30	2820	4491	6317	9639	3248	4449	6817	9791	1888	1999	3985	4361	12032	10927	9817	10753
31	551	1338	1589	3883	362	930	1810	3914	497	351	878	954	5886	6017	7284	7201
32	151	253	252	1085	70	152	335	1022	70	66	182	145	2302	2421	4034	2913
33	34	71	100	283	23	41	108	273	14	27	68	52	878	693	1513	1150
≥ 34	14	38	49	74	25	27	54	82	3	6	37	25	371	174	421	372
Total	36435	36435	36435	36435	36435	36435	36435	36435	36435	36435	36435	36435	36435	36435	36435	36435

Table 1 and Figure 5 show that the areas with temperatures between 27 – 30 °C are larger than the other temperatures. Low temperatures (≤ 26 °C) decreased relatively strongly in the area from 2001-2005 to 2006-2010, 2011-2015, and 2016-2020 (DJF, MAM, JJA), while SON was dominated by high temperatures 28-31 °C. The temperature composition of DJF like the MAM, namely the temperature of 27 °C decreases in the area from 7954 km² (DJF01-05) to 6365 km² (DJF06-10), 5879 km² (DJF11-15), and 2992 km² (DJF16-20); 6981 km² (MAM01-05) to 5131 km² (MAM06-10), 4240 km² (MAM11-15), and 2117 km² (MAM16-20). Similarly, at a temperature of 28 °C, the area decreases from 11589 km² (DJF01-05) to 12394 km² (DJF06-10), 10592 km² (DJF11-15), and 6531 km² (DJF16-20); from 13962 km² (MAM01-05) to 13777 km² (MAM06-10), 10427 km² (MAM11-15), and 7224 km² (MAM16-20). The area of 29 °C is relatively the same, while the temperature of 30 °C is wider, from 2820 km² (DJF01-05) to 4491 km² (DJF06-10), 6317 km² (DJF11-15), and 9639 km² (DJF16-20); from 3248 km² (MAM01-05) to 4449 km² (MAM06-10), 6817 km² (MAM11-15), and 9791 km² (MAM16-20). Similarly, it is larger for a temperature of 31 °C, from 551 km² (DJF01-05) to 1338 km² (DJF06-10), 1589 km² (DJF11-15), and 3883 km² (DJF16-20); from 362 km² (MAM01-05) to 930 km² (MAM06-10), 1810 km² (MAM11-15), and 3914 km² (MAM16-20). For high temperatures, namely 31, 32, 33, ≥ 34 °C, which is an increasingly common UHI for both DJF and MAM. JJA is dominated by a temperature of 28 °C, which tends to decrease in the area from the 2001-2005 mean to 2016-2020. In contrast, it tends to increase when temperatures range from 29 to 34 °C. In the low temperature season SON (≤ 28), is less pronounced compared to the seasons DJF, MAM, and JJA. The SON season is dominated by moderate (29 – 30 °C) and high (31, 32, 33, ≥ 34 °C) temperatures.

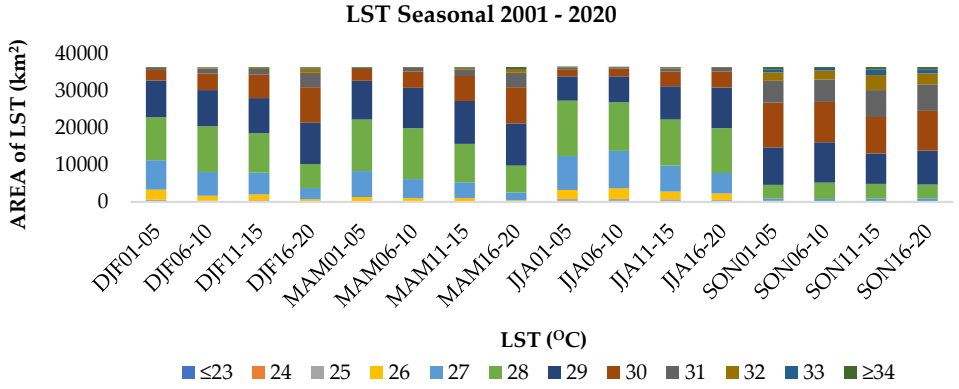

Figure 5. LST Seasonal (DJF, MAM, JJA, SON) 2001 – 2020.

3.1.2.2. LST area changes compared to 2001-2005

The LST area changes compared to 2001-2005 at the same temperature is calculated using Equation 1.

Preprints (www.preprints.org) | NOT PEER-REVIEWED | Posted: 30 May 2023 doi:10.20944/preprints202305.2099.v1

dSeason 06-10 = area (Season 2006-2010 – Season 2001-2005), (1a)
dSeason 11-15 = area (Season 2011-2015 – Season 2001-2005), (1b)
dSeason 16-20 = area (Season 2016-2020 – Season 2001-2005), (1c)
where:
d = delta = area changes = (km^2)
Season = area of DJF, MAM, JJA, and SON = (km^2)

Equation 1 yields the area of LST changes, as shown in Table 2 and Figure 6.

Table 2. LST area changes compared to 2001-2005

LST	LST AREA CHANGES COMPARED TO 2001-2005 (km^2)											
(°C)	dDJF 06-10	dDJF 11-15	dDJF 16-20	dMAM 06-10	dMAM 11-15	dMAM 16-20	dJJA 06-10	dJJA 11-15	dJJA 16-20	dSON 06-10	dSON 11-15	dSON 16-20
≤ 23	-35	-18	-38	-28	-33	-37	-2	-6	-27	0	0	2
24	-75	-42	-110	-83	-111	-131	-22	-65	-81	-2	-1	-2
25	-149	-101	-308	-235	-276	-383	33	-51	-186	-44	-34	-55
26	-1356	-1087	-2080	-1907	-1837	-2295	421	-332	-686	-98	-60	-57
27	-1589	-2075	-4962	-2823	-3704	-5837	985	-2094	-3578	59	151	254
28	805	-997	-5058	2188	-1162	-4365	-1842	-2540	-2832	724	237	10
29	-250	-466	1081	852	1527	1426	443	2403	4301	712	-1951	-1087
30	1671	3497	6819	1629	3997	6971	111	2097	2473	-1105	-2215	-1279
31	787	1038	3332	379	1259	3363	-146	381	457	131	1398	1315
32	102	101	934	1	184	871	-4	112	75	119	1732	611
33	37	66	249	7	74	239	13	54	38	-185	635	272
≥ 34	52	84	141	20	82	178	10	41	46	-311	108	16

From Table 2 and Figure 6, the area generally decreases at low temperatures (≤ 28 °C), whereas it increases at high temperatures (≥ 29 °C). LST ≤ 23, 24, 25 °C in all seasons and years, the area decreases between 2 and 383 km^2 except in JJA 06-10, when it increased by 33 km^2. LST 26 °C all seasons recorded a significant decrease in area (57 km^2 (SON 16-20) – 2295 km^2 (MAM 16-20)), except JJA 06-10, which expanded by 421 km^2. LST 27 °C all seasons experienced a significant decrease in area (1589 km^2 (DJF 06-10) to 5837 km^2 (MAM 16-20)), with the exception of JJA 06-10, which increased by 985 km^2 and SON (59 – 254 km^2). LST 28 °C more areas experienced a decrease in area, namely DJF 11-15, DJF 16-20, MAM 11-15, MAM 16-20, JJA 06-10, and JJA 11-15, JJA 16-20, while those that expanded during the season DJF 06-10, MAM 06-10, SON 06-10, SON 11-15, and SON 16-20. LST 29 °C, most seasons experience area expansion, except DJF 06-10, DJF 11-15, SON 11-16, and SON 16-20 experience area decline. LST 30 °C, all seasons experience area expansion. LST 31 and 32 °C, all seasons experience an area expansion except JJA 06-10. LST 33 and ≥ 34 °C, all seasons experience an area expansion except SON 06-10.

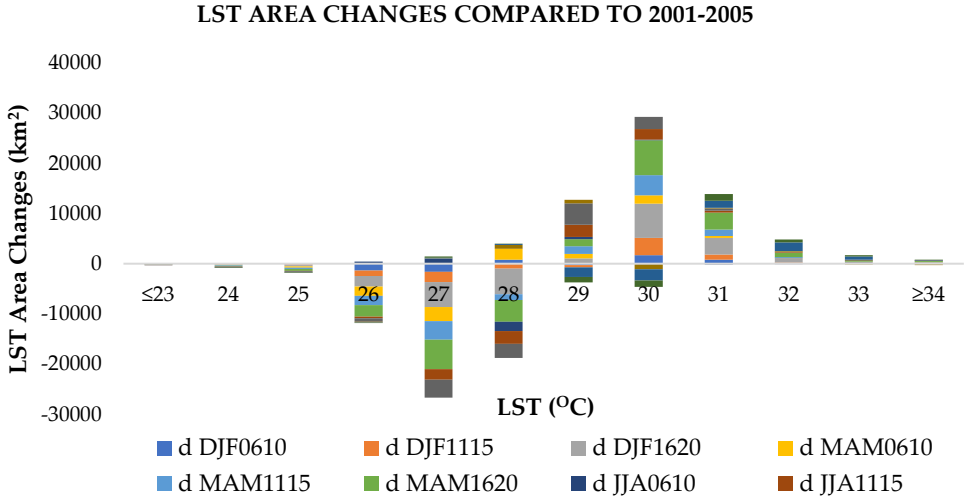

Figure 6. LST area changes compared to 2001-2005

Preprints (www.preprints.org) | NOT PEER-REVIEWED | Posted: 30 May 2023 doi:10.20944/preprints202305.2099.v1

3.2. LST Seasonal changes at the same location

3.2.1. Spatial analysis of LST Seasonal changes at the same location

To determine the changes of LST in the same location compared to 2001-2005, calculations are performed using Equation 2(a, b, c).

dLST season 06-10 = LST season 06-10 – LST season 01-15, (2a)

dLST season 11-15 = LST season 11-15 – LST season 01-15, (2b)

dLST season 16-20 = LST season 16-20 – LST season 01-15, (2c)

where:

d = delta/LST changes = (^{O}C)

LST season = LST DJF, MAM, JJA, and SON = (^{O}C)

The results of the calculation of Equation 2 are shown spatially in Figure 7. Temperature changes during the DJF season are shown in Figure 7(a, b, c), MAM in Figure 7(d, e, f), JJA in Figure 7(g, h, i), and SON in Figure 7(j, k, l). Temperature changes in ≤ -2 ^{O}C are shown in purple and blue, -1 light blue, 0 ^{O}C light green, 1 ^{O}C yellow, 2 ^{O}C orange, and ≥ 3 ^{O}C magenta.

Figure 7a (DJF 01-05 to DJF 06-10) shows positive temperature changes of 1, 2, ≥ 3 ^{O}C (yellow, orange, and magenta) around Samarinda, Balikpapan, Kutai Kertanegara Regency (west of Balikpapan), and North Penajam Paser Regency (PPU) in southern Balikpapan. In Figures 7b (DFJ 01-05 to 11-15) and 7c (DFJ 01-05 to 16-20), it can be seen that the area is expanding. The pattern of temperature increase in MAM (Figure 7d,e,f) and JJA in Figure 7 (g,h,i) is similar to DJF, but the areas of high temperature increase are not as large as in the DJF season. The pattern of temperature changes in SON season has a larger temperature decrease (-2 ^{O}C, blue color) than other seasonal patterns, which can be seen around Kutai Kertanegara district.

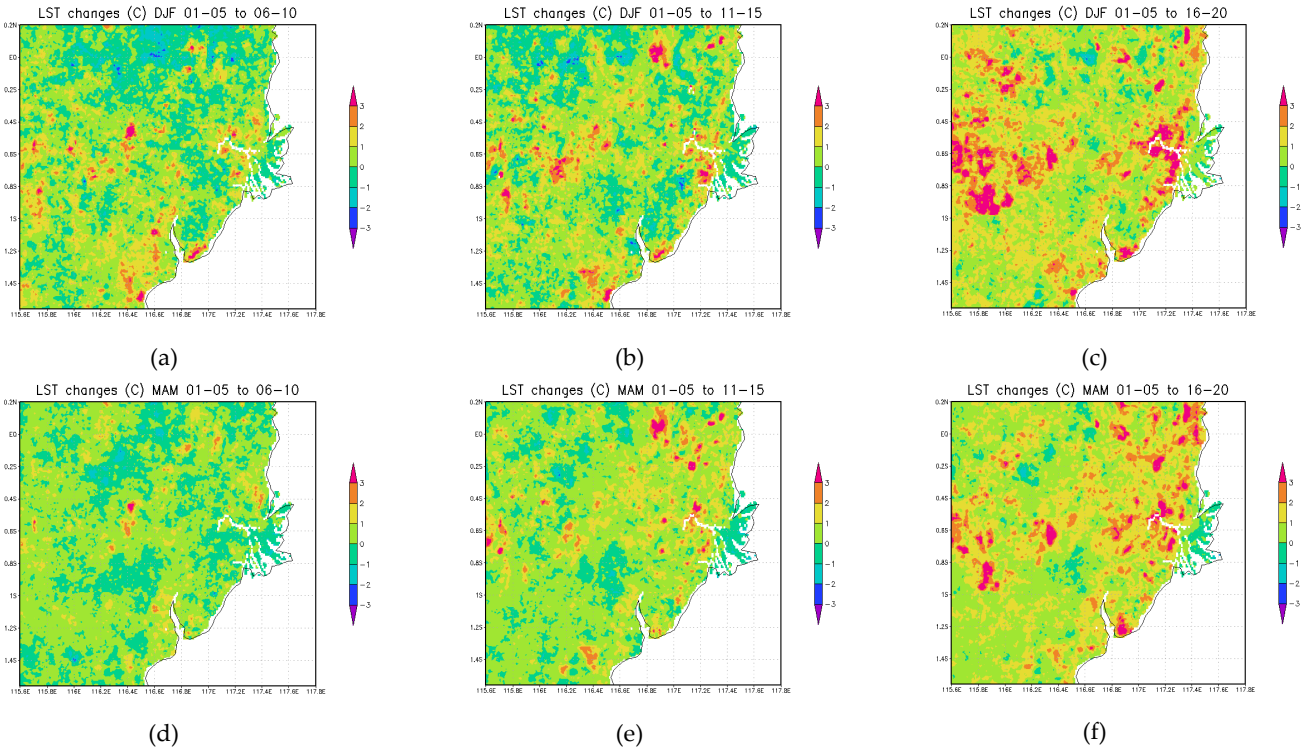

(a) (b) (c)

(d) (e) (f)

Preprints (www.preprints.org) | NOT PEER-REVIEWED | Posted: 30 May 2023 doi:10.20944/preprints202305.2099.v1

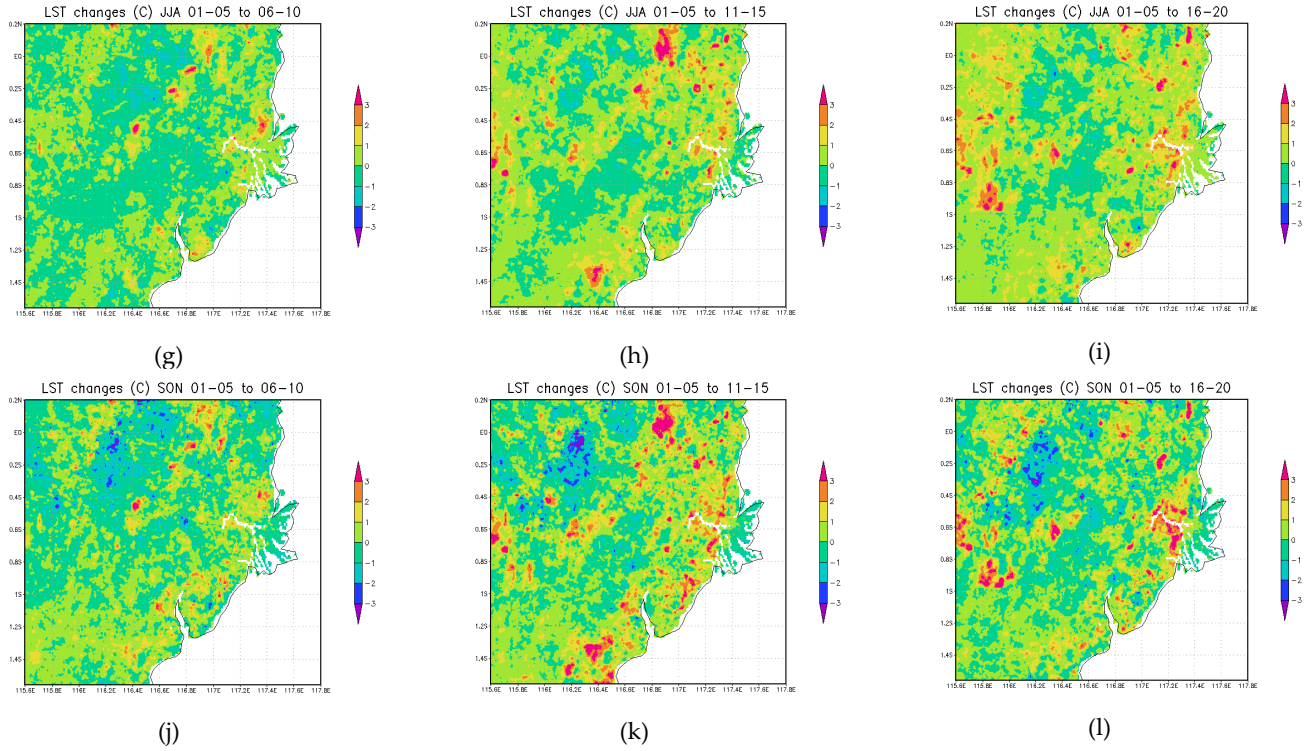

Figure 7. LST Seasonal changes in the same location, (a) DJF 2006-2010 – DJF 2001-2005, (b) DJF 2011-2015 - DJF 2001-2005, (c) DJF 2016-2020 – DJF 2001-2005, (d) MAM 2006-2010 – JJA 2001-2005, (e) MAM 2011-2015 - MAM 2001-2005, (f) MAM 2016-2020 – MAM 2001-2005, (g) JJA 2006-2010 – JJA 2001-2005, (h) JJA 2011-2015 – JJA 2001-2005, (i) JJA 2016-2020 – JJA 2001-2005, (j) SON 2006-2010 – SON 2001-2005, (k) SON 2011-2015 – SON 2001-2005, and (l) SON 2016-2020 – SON 2001-2005.

3.2.2. Statistical analysis of LST Seasonal changes at the same location

To determine the number of areas with temperature changes, a quantitative analysis is performed as shown in Table 3 and Figure 8 (dLST positive=increase, 0=constant, negatif=decrease). The locations where the temperature changes from largest to smallest are 1 ^{O}C (29657 km^2, yellow color in Figure 8); 0 ^{O}C (9212 km^2, gray); 2 ^{O}C (6826 km^2, light blue); 3 ^{O}C (1484 km^2, yellow), -1 ^{O}C (1005 km^2, orange); ≥4 ^{O}C (459 km^2, dark blue); and ≤-2 ^{O}C (65 km^2, blue).

Table 3. Area of LST changes (≤ -2 ^{O}C to ≥4 ^{O}C) at the same location

dLST (^{O}C)	AREA of LST changes (≤ -2 ^{O}C to ≥ 4 ^{O}C) at the same location (km^2)												
	DJF 06-10	DJF 11-15	DJF 16-20	MAM 06-10	MAM 11-15	MAM 16-20	JJA 06-10	JJA 11-15	JJA 16-20	SON 06-10	SON 11-15	SON 16-20	Ave-rage
≤ -2	119	94	36	8	5	6	22	4	24	456	5	2	65
-1	1582	1266	183	538	441	124	1745	772	736	4047	441	183	1005
0	11297	9921	2656	12006	7299	2400	18812	12003	8492	15697	7299	2656	9212
1	28787	29052	26934	33587	33886	29237	26211	30275	31696	25367	33886	26967	29657
2	5860	6653	13503	2357	5966	13169	1609	4376	6297	2651	5966	13503	6826
3	897	1385	3897	192	881	2943	247	976	1198	419	881	3897	1484
≥ 4	166	337	1499	20	230	829	62	302	265	71	230	1500	459

From 2001 to 2020, during the DJF season, sites that experienced temperature decreases (≤-2 and -1 ^{O}C) and those that remained constant (0 ^{O}C), tended to decrease in area, whereas temperature increases of 2, 3, and ≥4 ^{O}C led to expansion. In the MAM season, sites that experience a temperature decrease (-1 ^{O}C) and those that remain constant (0 ^{O}C) tend to decrease in area, while temperature increases of 2, 3, and ≥4 ^{O}C tended to result in expansion. During JJA season, sites that experience a temperature decrease in (-1 ^{O}C), as well as those that remain constant (0 ^{O}C), tend to decrease in area, while temperature increases of 1, 2, and 3 ^{O}C led to expansion. During the season SON, locations that experience a temperature decrease (≤-2 and -1 ^{O}C), as well as locations that remain

Preprints (www.preprints.org) | NOT PEER-REVIEWED | Posted: 30 May 2023 doi:10.20944/preprints202305.2099.v1

constant (0 ^{O}C), tend to decrease in area, while temperature increases of 1, 2, 3, and ≥4 ^{O}C lead to expansion.

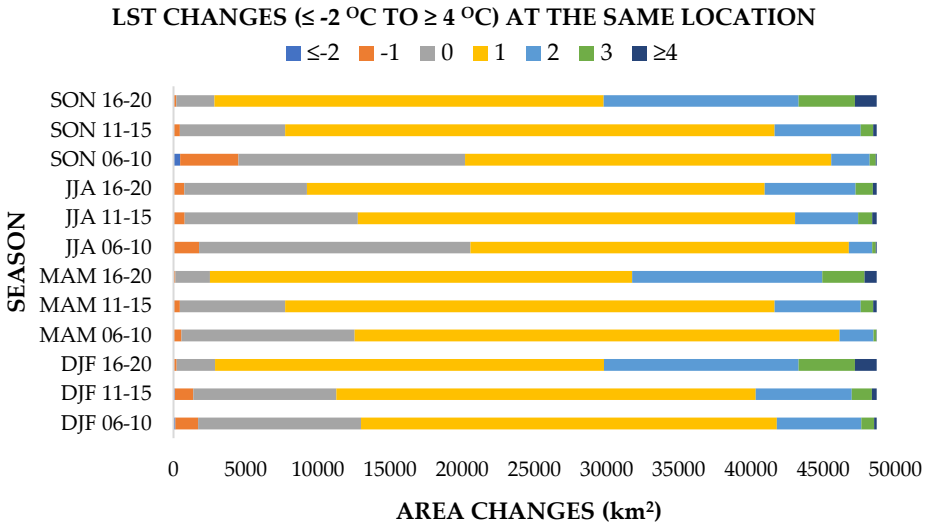

Figure 8. LST changes (≤ -2 ^{O}C to ≥ 4 ^{O}C) at the same location

3.3. LST analysis in Balikpapan, Samarinda, Bontang, and IKN zero point

3.3.1. LST Seasonal in Balikpapan, Samarinda, Bontang and IKN

To observe the comparison between LST at the IKN zero point (0.97S, 116.7E) and the urban areas as IKN buffer cities, namely Balikpapan City (1.24S, 116.85E), Samarinda City (0.49S, 117.18E) and Bontang City (0.12N, 117.46E), seasonal LST analysis is conducted at the 4 observation points as shown in Table 4 and Figure 9. From Table 4 and Figure 9, it can be seen that the sequence of LST from the lowest to the highest value is respectively at the IKN zero point, Bontang City, Samarinda City, and Balikpapan City. The lowest value of LST at the IKN zero point was reached in the seasons JJA 2001-2005 and JJA 2006-2010, namely 26.45 ^{O}C, while the highest value was reached in the season SON 2016-2020. Bontang had the lowest LST (29.96 ^{O}C) in JJA 2006-2010, and the highest (33.09 ^{O}C) in the MAM 2016-2020. Samarinda had the lowest LST (30.64 ^{O}C) in the MAM 2001-2005, while the highest (35.53 ^{O}C) was in MAM 2016-2020. The lowest LST (32.18 ^{O}C) in Balikpapan occurred in the JJA 2001-2005 season and the highest (37.91 ^{O}C) in SON 2016-2020.

Table 4. LST Seasonal in Balikpapan, Samarinda, Bontang and IKN zero point

CITY	LST SEASONAL (^{O}C)															
	DJF 01-05	DJF 06-10	DJF 11-15	DJF 16-20	MAM 01-05	MAM 06-10	MAM 11-15	MAM 16-20	JJA 01-05	JJA 06-10	JJA 11-15	JJA 16-20	SON 01-05	SON 06-10	SON 11-15	SON 16-20
Balikpapan	35.35	36.95	36.38	36.84	33.98	35.67	34.13	36.80	32.18	32.60	32.24	32.22	35.80	35.13	36.01	37.91
Samarinda	30.18	32.98	33.66	36.13	30.82	31.63	32.48	35.53	30.64	30.68	31.77	33.02	33.28	33.22	33.48	35.36
Bontang	31.03	31.25	31.91	32.30	31.30	31.25	31.47	33.09	30.20	29.96	29.76	30.14	31.96	31.33	31.52	31.66
IKN 0 point	27.30	28.82	27.71	28.82	27.05	27.89	28.19	28.61	26.45	26.45	27.20	27.55	28.47	29.56	29.77	30.04

Preprints (www.preprints.org) | NOT PEER-REVIEWED | Posted: 30 May 2023 doi:10.20944/preprints202305.2099.v1

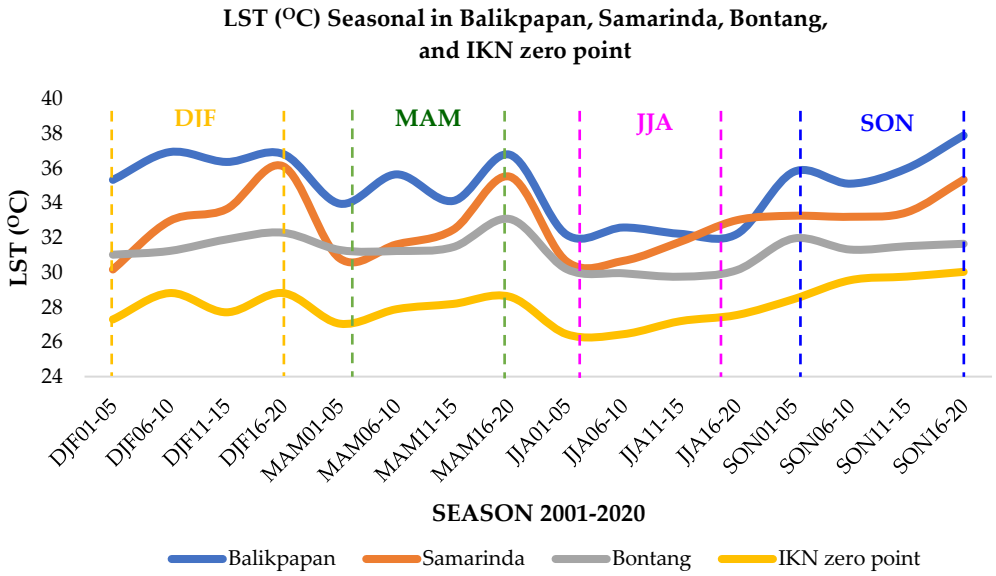

Figure 9. LST Seasonal in Balikpapan, Samarinda, Bontang and IKN zero point

3.3.2. Cross-sectional analysis of the LST

Cross-section analysis was conducted to observe the UHI pattern in two dimensions. Cross-sections are conducted by drawing lines from north to south (latitudinal) and west to east (longitudinal) through the observation points, namely the cities of Balikpapan, Samarinda, Bontang, and the IKN zero point. In this study, the cases of DJF 2016-2020 season cases were selected as shown in Figure 10.

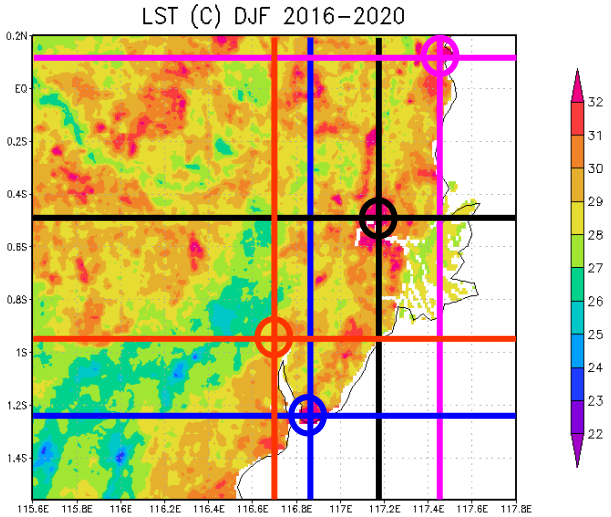

Figure 10. Cross-section of LST DJF 2016-2020 in 4 places: Bontang City (purple circle), Samarinda City (black circle), IKN zero point (red circle), and Balikpapan City (blue circle).

The results of cross-section data processing are presented graphically in Figure 11. For UHI analysis, LST data is needed in Table 4. The LST of DJF 2016-2020 season for Balikpapan City is 36.84 °C, Samarinda City 36.13 °C, Bontang City 32.3 °C, and IKN zero-point 28.82 °C. Figures 11(a) and (b) are latitudinal and longitudinal cross-sections of Balikpapan City. Here it can be seen that Balikpapan City (blue circle) has the highest temperature (36.84 °C) compared to the surrounding areas. This indicates that Balikpapan City is the center of UHI. The Samarinda City (black circle) in Figure 11 (c, d) also shows that UHI is present with a high temperature (36.13 °C) compared to the surrounding area.

Preprints (www.preprints.org) | NOT PEER-REVIEWED | Posted: 30 May 2023 doi:10.20944/preprints202305.2099.v1

In Figure 11(e, f), the UHI is shown in Bontang City, with a high temperature of 32.3 ^{O}C. Unlike the graphs for the 3 previous cities, Figure 11(g, h) shows a lower temperature (28.82 ^{O}C) for the IKN zero point. This indicates that UHI has not occurred in the IKN area.

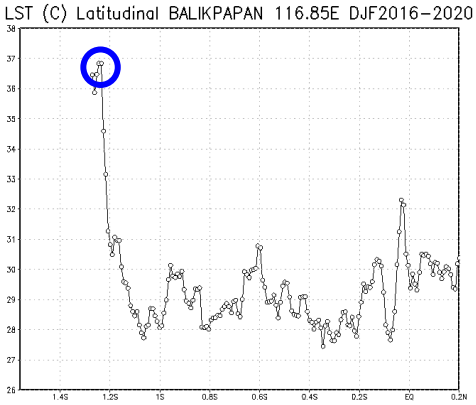

(a)

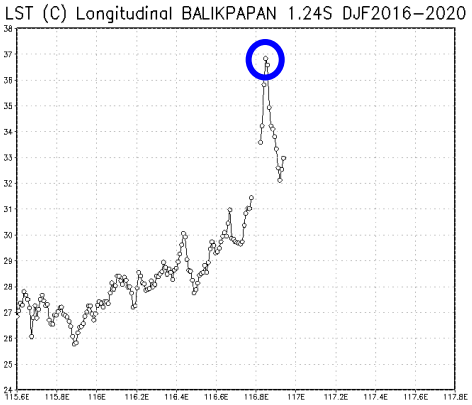

(b)

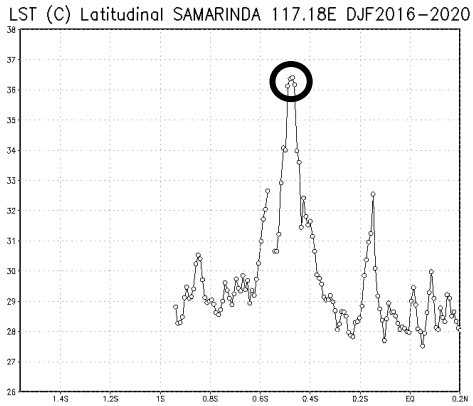

(c)

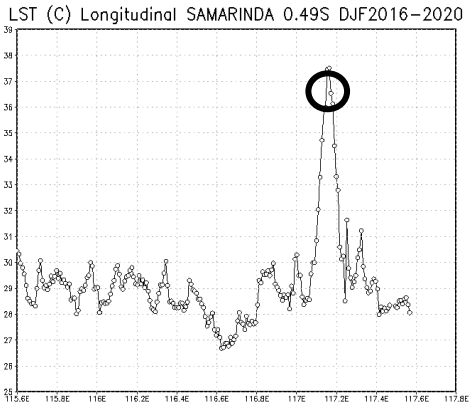

(d)

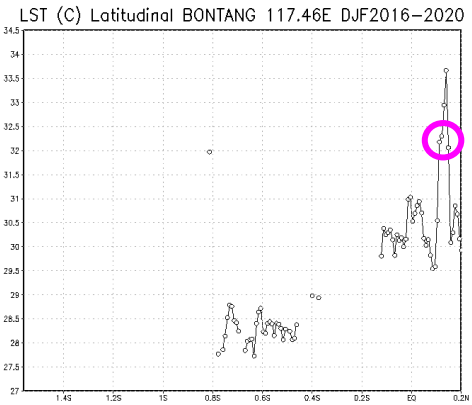

(e)

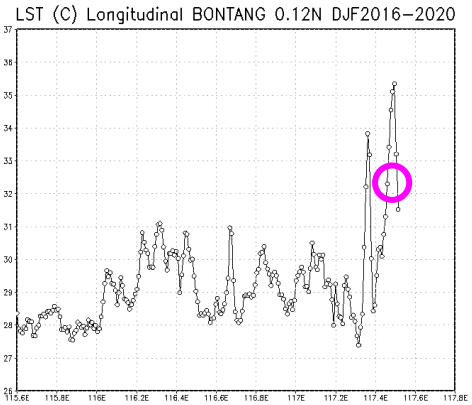

(f)

Preprints (www.preprints.org) | NOT PEER-REVIEWED | Posted: 30 May 2023 doi:10.20944/preprints202305.2099.v1

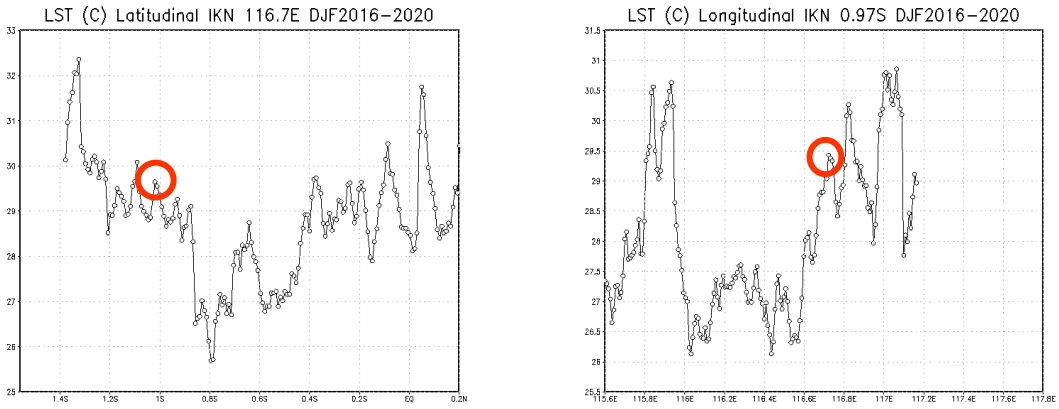

(g) (h)

Figure 11. Graphics of Cross Section LST DJF 2016-2020 in 4 places, namely Balikpapan City (blue circle) latitudinal (a) and longitudinal (b); Samarinda City (black circle) latitudinal (c) and longitudinal (d); Bontang City (purple circle) latitudinal (e) and longitudinal (f); and IKN zero point (red circle) latitudinal (g) and longitudinal (h).

4. Discussions

The highest temperatures in East Kalimantan occur during the SON season, otherwise lowest temperature during JJA season. This is because East Kalimantan Province is one of 38 provinces in Indonesia which is located in the tropics and is crossed by the equator. With this geographical location, the sun will cross East Kalimantan twice a year, the first in February to April and the second in September to November [23,24], on 21 March and 23 September, the sun is directly above the equator.

For high temperatures, namely 31, 32, 33, ≥ 34 ^{O}C, which represents UHI which is increasingly widespread UHI both in the DJF and MAM seasons. JJA is dominated by a temperature of 28 ^{O}C which tends to decrease in the area from the average of 2001-2005 to 2016-2020. Conversely, for temperatures of 29 – 34 ^{O}C it tends to expand. In the low-temperature SON season (≤ 28) it is less extensive compared to the DJF, MAM, and JJA seasons. The SON season is dominated by moderate (29 – 30 ^{O}C) and high (31, 32, 33, ≥ 34 ^{O}C) temperatures. UHI in the study area has occurred in three buffer cities in East Kalimantan (Balikpapan City (36.84 ^{O}C), Samarinda City (36.13 ^{O}C), and Bontang City (32.3 ^{O}C)) respectively from high to low LST. In the cities, urbanization replaces vegetation that minimal amounts of water for evapotranspiration in urban areas[25]. In the urban area of Beijing, the measured soil heat flux is 50% of the total net radiation [26]. High LST in urban areas will increase the instability of the air on the asphalt and will directly heat the air and increase the air temperature [27]. UHI is located in the downtown area where there are many buildings. Green surfaces can reduce the effect of UHI, while built-up areas can strengthen UHI [28]. Reducing the latent heat flux in urban areas on impermeable surfaces will reduce the transfer of moisture from the soil to the atmosphere [29]. The seasonal trends of LST with higher LST are mainly concentrated in industrial and business districts [30]. The IKN zero point has the lowest temperature (28.82 ^{O}C) among the 3 buffer cities of IKN, which means UHI has not yet occurred, this is because during the observation period (2001-2020) IKN is still a vegetated mountain planted with *Acacia mangium* and *Eucalyptus sp*. Reduced evaporation will warm the ground and air surface, thereby increasing the sensible heat flux [29] and reducing the convenience of urban living. It is very important to maintain the condition of IKN which is still vegetated and UHI has not yet occurred. As a mitigation effort, for IKN development, it is necessary to choose building materials that can reduce the effects of UHI, including white roofs [29,31,32]

While the other 3 cities are areas that have long been developing. Bontang is an oriented city in the fields of industry, services, and trade, standing 3 large companies in

 doi:10.20944/preprints202305.2099.v1

the fields of natural gas, fertilizers, and coal. Samarinda is the capital city of East Kalimantan province with the largest population in East Kalimantan, with two of the busiest ports in East Kalimantan (Samarinda Port and Palaran Port). Balikpapan is the most populous city in East Kalimantan (2190 people/km^2), as a center for business and industry (oil, gas, coal, and palm oil), there is an international airport and two seaports. In mountainous areas, the LST is lower than in urban areas because the surface incoming solar radiation will be weaker [33,34].

For future research, several factors related to UHI will be examined, namely Land Use and Land Cover Change (LULCC) [2,29,30], Normalized Difference Built-Up Index (NDBI) [35], Albedo, Normalized Difference Vegetation Index (NDVI) [36,37], anthropogenic heat and Comfortable Index [38–40], Normalized Difference Water Index (NDWI) [31,36], and Air Pollution [41–43].

5. Conclusions

From the results of the research and analysis above, discussing LST on a seasonal basis will make it easier to observe UHI dynamics. Using GEE as a web-based platform is very helpful for processing remote sensing data [9–13], in this study as a tool for estimating LST. UHI (high LST) propagation has occurred in the urban areas of Balikpapan, Samarinda, and Bontang, East Kalimantan. However, at the IKN zero point, there is no visible UHI, this should be maintained. A more in-depth study of the climate and environmental conditions of the IKN is needed to support the strategic program for the development of the IKN with the concept of Forest City and Climate Plus Village (Proklim+). In the end, IKN hopes to become a smart metropolis that guarantees the highest quality of life for its residents. The condition of IKN that has not yet occurred UHI needs to be maintained so that it supports sustainable development goals (SDGs) 11th (sustainable cities and communities), 13th (Climate Action), and 15th (Life on Land). The results of this study are useful for policy makers and urban planner as one of the scientific considerations in the city development especially in the IKN.

Supplementary Materials: Not Applicable.

Author Contributions: Conceptualization, Laras Tursilowati (primary contributor); Data curation, Rachmat Sunarya and Muzirwan Muzirwan; Formal analysis, Laras Tursilowati; Methodology, Laras Tursilowati and Indah Susanti; Project administration, Laras Tursilowati; Resources, Jamrud Aminuddin and Nursida Arif; Software, Laras Tursilowati, Indah Susanti and Mamat Suhermat; Supervision, Laras Tursilowati; Validation, Soni Rahayu and Tatik Kartika; Visualization, Laras Tursilowati, Indah Susanti and Mamat Suhermat; Writing – original draft, Laras Tursilowati, Rachmat Sunarya, Muzirwan Muzirwan, Indah Susanti, Soni Rahayu, Tatik Kartika, Mamat Suhermat, Jamrud Aminuddin and Nursida Arif; Writing – review & editing, Laras Tursilowati.

Funding: This research received no external funding.

Data Availability Statement: Not Applicable.

Acknowledgments: The authors would like to thank the National Research and Innovation Agency (BRIN) which has provided the facilities we needed to conduct research. The author would also like to thank the Climate Change group who assisted in the analysis and discussion.

Conflicts of Interest: The authors declare no conflict of interest.

References

1. Urgensi Pemindahan Ibu Kota Negara. Available online: https://www.djkn.kemenkeu.go.id/kanwil-kalbar/baca-artikel/14671/Urgensi-Pemindahan-Ibu-Kota-Negara.html (accessed on 9 January 2023).
2. Aslan, N. and Koc-San, D. Analysis of Relationship between Urban Heat Island Effect and Land Use/Cover Type using LANDSAT 7 ETM+ and LANDSAT 8 OLI Images. In Proceeding of The International Archives of the Photogrammetry, Remote Sensing and Spatial Information Sciences, XL-B8. Prague, Czech Republic, 12-19 July 2016, doi:10.5194/isprsarchives-XLI-B8-821-2016.

3. Connors, J. P.; Galletti, C. S. and Chow, W. T. L. Landscape configuration and urban heat island effects: assessing the relationship between landscape characteristics and land surface temperature in Phoenix, Arizona. *Landscape Ecology* **2013**, *28*, 271–283, Springer, DOI 10.1007/s10980-012-9833-1.
4. McCarthy, M. P.; Best, M. J. and Betts, R. A. Climate change in cities due to global warming and urban effects, *Geophysical Research Letters* **2010**, *37*, L09705, doi:10.1029/2010GL042845.
5. Azevedo, J.A.; Chapman, L. and Muller, C. L. Quantifying the Daytime and Night-Time Urban Heat Island in Birmingham, UK: A Comparison of Satellite Derived Land Surface Temperature and High Resolution Air Temperature Observations. *Remote Sensing* **2016**, *8*, 153, doi:10.3390/rs8020153.
6. Chapman, S.; Thatcher, M.; Salazar, A.; Watson, J. E. and McAlpine, C. A. The Effect of Urban Density and Vegetation Cover on the Heat Island of a Subtropical City. *Journal of Applied Meteorology and Climatology* **2018**, *57(11)*, 2531-50.
7. Tursilowati, L.; Sumantyo, J. T. S.; Kuze, H. and Adiningsih, E. S. The integrated WRF/urban modeling system and its application to monitoring urban heat island in Jakarta, Indonesia. *Journal of Urban and Environmental Engineering (JUEE)* **2012**, *6(1)*, 1-9 ISSN 1982-3932, doi:10.4090/juee.2012.v6n1.001009.
8. Denryanto, R. A. F. and Virgianto, R. H. The impact of land cover changes on temperature parameters in new capital of Indonesia (IKN). In Proceeding of the 2nd International Conference on Tropical Meteorology and Atmospheric Sciences, IOP Conference Series: Earth and Environmental Science **2021**. *893 012033*, doi:10.1088/1755-1315/893/1/012033.
9. Jaelani, L. M. and Handayani, S. A. Spatio-temporal Analysis of Land Surface Temperature Changes in Java Island from Aqua and Terra MODIS Satellite Imageries Using Google Earth Engine. *International Journal of Geoinformatics* **2022**, *18(5)*, 1-12, https://doi.org/10.52939/ijg.v18i5.2365.
10. Lodato, F.; Colonna, N.; Pennazza, G.; Praticò, S.; Vollero, L. and Pollino, M. Analysis of the Spatiotemporal Urban Expansion of the Rome Coastline through GEE and RF Algorithm, Using Landsat Imagery. *ISPRS International Journal of Geo-Information* 2023, *12 (141)*, 1-25, https://doi.org/10.3390/ijgi12040141.
11. Ravanelli, R.; Nascetti, A.; Cirigliano, R. V.; Di Rico, C.; Monti, P. and Crespi, M. Monitoring Urban Heat Island through Google Earth Engine: Potentialities and Difficulties in Different Cities of The United States. *The International Archives of the Photogrammetry, Remote Sensing and Spatial Information Sciences* **2018**, XLII-3, 1467-1472, https://doi.org/10.5194/isprs-archives-XLII-3-1467-2018.
12. Sunarta, I. N.; Suyarto, R.; Saifulloh M.; Wiyanti, W.; Susila, K. D. and Kusumadewi, L. G. L. Surcafe Urban Heat Island (SUHI) Phenomenon in Bali and Lombok Tourism Areas based on Remote Sensing. *Journal of Southwest Jiaotong University* **2022**, *57 (4)*, 504-521, doi:10.35741/issn.0258-2724.57.4.44.
13. Zafrir, R.; Ojeda, S.; Singh, H. and Hahn, M. Seasons in Stuttgart: Developing a Google Earth Engine Tool for Heat Island Mapping. In Proceeding of The International Archives of the Photogrammetry, Remote Sensing and Spatial Information Sciences, Karaj, Iran, 12-14 October 201, https://doi.org/10.5194/isprs-archives-XLII-E-W18-1123-2019.
14. East Kalimantan, Indonesia Climate. Available online: https://tcktcktck.org/indonesia/east-kalimantan (accessed on 19 February 2023)
15. Samarinda Annual Weather Averages. Available online: https://www.worldweatheronline.com/samarinda-weather-averages/east-kalimantan/id.aspx (accessed on 12 February 2023).
16. Climate & Weather Averages in Balikpapan, East Kalimantan, Indonesia. Available online: https://www.timeanddate.com/weather/indonesia/balikpapan/climate (accessed on 19 February 2023)
17. Statistics Kalimantan Timur. Available online: https://kaltim.bps.go.id/indicator/151/287/1/air-temperature-by-month-in-balikpapan.html (accessed on 19 February 2023). Source: Meteorology and Geophysics Board
18. MOD11A1-MODIS/Terra Land Surface Temperature/Emissivity Daily L3 Global 1km SIN Grid. Available online: https://ladsweb.modaps.eosdis.nasa.gov/missions-and-measurements/products/MOD11A1 (accessed on 15 February 2023)
19. Wan, Z, *Modis Land-Surface Temperature Algorithm Theoretical Basis Document (LST ATBD)*, Version 3.3; Institute for Computational Earth System Science, University of California, Santa Barbara, 2013; pp. 1-77.
20. Wan, Z, *Collection-6 MODIS Land Surface Temperature Products Users' Guide*; ERI, University of California, Santa Barbara, 2013; pp. 1-33.
21. Network Common Data Form (NetCDF). Available online: https://www.unidata.ucar.edu/software/netcdf/ (accessed on 10 January 2023).
22. GrADS, Grid Analysis and Display System George Mason University. Available online: http://cola.gmu.edu/grads/ (accessed on 20 January 2023).
23. Winarno, G. D.; Harianto, S. P. and Santoso, T. *Klimatologi Pertanian*; Pusaka Media: Bandarlampung, Indonesia, 2019; pp xii+134
24. Pulihasih, A. Y. and Sujalu, A. P. The Dynamics of Rain Pattern in East Kalimantan. *International Journal of Environment and Climate Change* **2022**, *12*(11), 14-18, Article no.IJECC.88670, DOI: 10.9734/IJECC/2022/v12i1130938.
25. Helfer, F.; Lemckert, C. and Zhang, H. Impacts of climate change on temperature and evaporation from a large reservoir in Australia, *Journal of Hydrology* **2012**, *475*, 365-378, Elsevier. http://dx.doi.org/10.1016/j.jhydrol.2012.10.008. www.elsevier.com/locate/jhydrol
26. Wang, K.; Jiang, S.; Wang, J.; Zhou, C.; Wang, X. and Lee, X. Comparing the diurnal and seasonal variabilities of atmospheric and surface urban heat islands based on the Beijing urban meteorological network. *Journal of Geophysical Research: Atmospheres* **2017**, *122*, 2131-2154, doi:10.1002/2016JD025304.
27. Gonçalves, A.; Ornellas, G.; Ribeiro, A. C.; Maia, F.; Rocha, A. and Feliciano. Urban Cold and Heat Island in the City of Bragança (Portugal). *Climate* **2018**, *6*(70), 1-14, doi:10.3390/cli6030070.

28. Ambrose, Z.A.; Abbas, B. and Asa, S. The Effects of Urban Parameters on the Development of Urban Heat Island in Jalingo Metropolis: Analysis and Statistical Modeling. Jalingo Journal of Social and Management Sciences **2019**, *1*(4), 146-165.
29. Jacobson, M. Z. and Ten Hoeve, J. E. Effects of Urban Surfaces and White Roofs on Global and Regional Climate, *Journal of Climate* **2011**, *25*, 1028-1044, American Meteorological Society. DOI: 10.1175/JCLI-D-11-00032.1.
30. Miao, S. G.; Dou, J. C.; Chen, F.; Li, J. and Li, A.G. An assessment of storage terms in the surface energy balance in Beijing **2012**, *55*(11), 1881-1890, doi:10.1007/s11430-012-4411-6.
31. Elsayed, I. S. M. Mitigation of the Urban Heat Island of the City of Kuala Lumpur, Malaysia. *Middle-East Journal of Scientific Research* **2012**, *11*, 1602-1613, ISSN 1990-9233, DOI: 10.5829/idosi.mejsr.2012.11.11.1590.
32. Kerns, B. K.; Powell, D. C.; Mellmann-Brown, S.; Carnwath, G. and Kim, J. B. Effects of projected climate change on vegetation in the Blue Mountains ecoregion, USA. *Climate Service* **2017**, 33-43, http://dx.doi.org/10.1016/j.cliser.2017.07.002.
33. Qiao, Z.; Tian, G.; Zhang, L. and Xu, X. Influences of Urban Expansion on Urban Heat Island in Beijing during 1989-2010. *Advances in Meteorologi* **2014**, Article ID 187169, 11 pages. http://dx.doi.org/10.1155/2014/187169.
34. Yuan, Y.; Xi, C.; Jing, Q. and Felix, N. Seasonal Variations of the Urban Thermal Environment Effect in a Tropical Coastal City. *Advances in Meteorology* **2017**, *ID 8917310*, 18 p, https://doi.org/10.1155/2017/8917310.
35. Renard, F.; Alonso, L.; Fitts, Y.; Hadjiosif, A. and Comby, J. Evaluation of Effect of Urban Redevelopment on Surface Urban Heat Islands. *Remote Sensing* **2019**, *11 (299)*, 1-31, doi:10.3390/rs11030299.
36. Prasasti, I.; Suwarsono and Sari, N. M. The Effect of Environmental Condition Changes on Distribution of Urban Heat Island in Jakarta based on Remote Sensing Data. *International Journal of Remote Sensing and Earth Science* **2015**, *12*, 27-40.
37. Effat, H. A. and Hassan, O. A. K. Change detection of urban heat islands and some r elated parameters using multi-temporal Landsat images; a case study for Cairo city, Egypt. *Urban Climate* **2014**, *10*, 171-188, http://dx.doi.org/10.1016/j.uclim.2014.10.011.
38. Betancourt, R. M. and Nenes, A. Understanding the contributions of aerosol properties and parameterization discrepancies to droplet number variability in a global climate model. *Atmos. Chem. Phys*. **2014**, *14*, 4809–4826, doi:10.5194/acp-14-4809-2014. www.atmos-chem-phys.net/14/4809/2014/.
39. Mohan M, Gupta A and Bhati S. A modified approach to analyze thermal comfort classification. *Atmospheric and Climate Sciences* **2014**, *4*, 7-11. http://dx.doi.org/10.4236/acs.2014.41002.
40. Toersilowati, L.; Siswanto, B.; Maryadi, E.; Susanti, I.; Suhermat, M.; Witono, A.; Sipayung, S. B.; Rahayu, S. A.; 'Adany, S.; Aminuddin, J. and Lubis, R. F. The Projections of Climate Change using Conformal Cubic Atmospheric Model (CCAM) in Bali – Indonesia. In Proceedings of IOP Conf. Series: Earth and Environmental Science, Bandung, Indonesia, 9 December 2021. 1047 (2022) 012033, doi:10.1088/1755-1315/1047/1/012033.
41. Zheng, Y. and Weng, Q. High spatial- and temporal-resolution anthropogenic heat discharge estimation in Los Angeles County, California. *Journal of Environmental Management* **2017**, Elsevier. http://dx.doi.org/10.1016/j.jenvman.2017.07.047.
42. Fitriani, A.N.; Dewi, K. and Tursilowati, L. Identification of Urban Heat Island Spreading Concentration of NO_2, O_3, and PM_{10} Pollutant in DKI Jakarta. *Journal of Urban and Environmental Engineering* **2019**, *13(1)*, 125-133, ISSN 1982-3932, doi: 10.4090/juee.2019.v13n1.125133.
43. Xu, L. Y.; Xie, X. D. and Li, S. Correlation analysis of the urban heat island effect and the spatial and temporal distribution of atmospheric particulates using TM images in Beijing. *Environmental Pollution* **2013**, *178*102-114, https://doi.org/10.1016/j.envpol.2013.03.006/